Radio Science®

METHOD

10.1029/2025RS008417

Artificial Intelligence Weather Radar

Jothiram Vivekanandan[1] and **Gwo-Jong Huang**[1]

[1]Earth Observing Laboratory, National Center for Atmospheric Research (NCAR), Boulder, CO, USA

Abstract The integration of artificial intelligence (AI) with weather radar systems marks a transformative advancement in remote sensing. This study introduces an AI-powered radar system that utilizes Long Short-Term Memory (LSTM) neural networks to predict the in-phase (I) and quadrature (Q) components of radar signals, enabling faster, and more accurate radar observations By synthesizing extended time series from a subset of real-time measurements, the AI radar enhances measurement accuracy and spatial resolution without requiring longer dwell times. The proposed technique reduces data collection time and storage demands while maintaining the statistical and spectral characteristics of radar signals. Applied to both simulated and measured radar data, the AI radar demonstrates promising results in improving signal prediction and radar observations across ground-based, airborne, and spaceborne platforms. This innovation paves the way for more efficient radar technologies, with potential applications in weather monitoring, military systems, and resource-constrained environments.

Plain Language Summary This paper introduces a new artificial intelligence (AI)-powered radar system that uses machine learning to improve weather monitoring. Traditional radars require a significant amount of time and data to provide accurate measurements, but the AI radar utilizes a neural network called Long Short-Term Memory to predict extended radar signals. By combining real-time measurements with predicted data, the system generates longer and more detailed radar observations, eliminating the need for additional time or resources. This approach enhances accuracy, speeds up data collection, and applies to various radar platforms, including ground-based, airborne, and spaceborne systems. The technology could be useful for weather forecasting, research, and even military applications.

Key Points:

- AI radar utilizes Long Short-Term Memory (LSTM) neural networks to predict radar *I*/*Q* signals, thereby enhancing the speed and accuracy of radar observations
- Existing radar with an LSTM network boosts spatial resolution and accuracy of measurements without increasing the data collection period
- The technique is applicable across ground, airborne, and spaceborne radar systems, with applications in a wide range of remote sensing

Correspondence to:

J. Vivekanandan,
vivek@ucar.edu

Citation:

Vivekanandan, J., & Huang, G.-J. (2025). Artificial intelligence weather radar. *Radio Science*, *60*, e2025RS008417. https://doi.org/10.1029/2025RS008417

Received 7 JUL 2025
Accepted 30 NOV 2025

Author Contributions:

Conceptualization: Jothiram Vivekanandan
Formal analysis: Jothiram Vivekanandan, Gwo-Jong Huang
Investigation: Jothiram Vivekanandan
Methodology: Jothiram Vivekanandan
Project administration: Jothiram Vivekanandan
Resources: Jothiram Vivekanandan
Software: Jothiram Vivekanandan, Gwo-Jong Huang
Supervision: Jothiram Vivekanandan
Validation: Jothiram Vivekanandan
Visualization: Jothiram Vivekanandan
Writing – original draft: Jothiram Vivekanandan
Writing – review & editing: Jothiram Vivekanandan

1. Introduction

A pulse Doppler radar transmits a series of pulses at pulse repetition time (PRT), T_s. Radar transmits at a carrier frequency offset by an intermediate frequency (IF). Weather radar detects backscatter from hydrometeors, including raindrops, ice crystals, and snowflakes. The low noise amplifier (LNA) amplifies the weak back-scattered signal in the receiver subsystem. The signal from LNA is mixed with a carrier frequency to down-convert to IF to detect the received signal using a matched filter. Subsequently, the IF received signals are mixed down to the baseband and split into I and Q components using the sine and cosine of the IF. I and Q signals are digitized by analog-to-digital converters (ADCs). The letter "I" stands for in-phase, and "Q" stands for quadrature components of the received signal (Bringi & Chandrasekar, 2001). The I and Q components are the root signal or "level 0 measurement" for all the downstream radar estimates, namely, reflectivity (signal power), radial velocity, and Doppler spectrum width (Crum et al., 1993). The mean and standard error in the estimate of weather radar measurements are time-averaged parameters derived from the I and Q time series.

The PRT and wavelength (λ) of a radar system are fundamental parameters that determine the unambiguous range (R_a) and Nyquist Doppler velocity (V_n). The maximum unambiguous range is the farthest distance at which a radar can unambiguously determine the location of a target without range folding (aliasing). It depends on the PRT. The Nyquist velocity is the maximum unambiguous radial velocity that a Doppler radar can measure without velocity aliasing. It depends on the wavelength (λ) and PRT. The PRT, λ, scan rate, and number of received samples are critical parameters in weather radar systems that directly influence radar resolution volume (i.e., the smallest detectable atmospheric region) and measurement accuracy. Resolution volume in its basic geometric form is a function of antenna beamwidth, radar pulse width, and range from the radar, and it is independent of scan rate or number of radar signal samples. However, the number of radar signal samples, which depends on PRT and scan rate, affects the signal-to-noise ratio and measurement accuracy of radar within the radar resolution volume (Doviak & Zrnic, 2014).

The scan rate is the speed at which the radar beam covers a specified angular sector of the atmosphere. Scan rate and the number of samples (N) critically impact weather radar measurements of SNR, Doppler velocity (V_r), and spectrum width (σ_v). Dwell time (T_D) is the duration for which the radar beam scans a specified angular sector. Faster scan rates reduce T_D, decreasing the number of samples (N) and lowering SNR ($\propto\sqrt{N}$), while also increasing velocity error ($V_{\sigma_v} \propto 1/(T_D\sqrt{N})$) and spectrum width uncertainty ($\sigma_s \propto V_n/\sqrt{N}$) (Doviak & Zrnic, 2014). Longer dwell times allow for the collection of more I/Q samples. Slow scans improve accuracy by allowing more samples, but delay data updates. A faster scan rate is desirable for covering a larger sector in a shorter time. Still, it can come at the cost of fewer I/Q samples per pixel, potentially degrading the quality of radar measurements. Adaptive techniques, such as staggered PRT and phased-array beam steering, optimize these trade-offs, prioritizing fast scans for severe weather (e.g., tornadoes) and slow, high-N scans for precipitation quantification. Advanced processing (e.g., pulse-pair or spectral averaging) further mitigates limitations, balancing resolution, accuracy, and update rates of radar measurements (Zhang, 2016). The relation between scan rate and number of samples is particularly critical in airborne and spaceborne systems, where the platform is in motion and the dwell time available to measure signals from a specified angular sector is limited.

Accurate radar measurements of precipitation and wind fields are fundamentally limited by trade-offs between spatial resolution, temporal sampling, and signal-to-noise ratio (SNR). Recent advances in AI machine Learning (ML) offer promising solutions for predicting in-phase/quadrature (I/Q) radar samples based on real-time radar measurements. This study investigates the potential of I/Q sample prediction to break existing performance trade-offs, presenting a framework that could redefine the boundaries of radar remote sensing for atmospheric observations. Section 2 describes weather radar signals and the simulation of I/Q. Rationale for predicting I/Q is presented in Section 3. Section 4 describes a technique for predicting the I/Q and conceptual process flow of AI weather radar. Validation of I/Q prediction using a simulated weather signal with a neural network and its application to weather radar measurements is presented in Section 5. A summary of concluding remarks was presented in Section 6.

2. Background on Radar Signals

Hydrometeors are randomly distributed within the radar sampling volume. According to the central limit theorem, the radar echo represents the sum of backscattered signals from a large number of randomly distributed hydrometeors, resulting in a Gaussian random variable. The backscattered radar signal from a precipitation volume is random in amplitude and phase because it is an ensemble of individual hydrometeors of various sizes and randomly located within a radar resolution volume (Zhang, 2016). The in-phase (I) and quadrature (Q) components of narrowband weather radar signals are zero-mean, jointly Gaussian random variables with equal variance (σ^2) and are typically uncorrelated. The signal amplitude ($A = \sqrt{(I^2 + Q^2)}$) typically follows a Rayleigh distribution for precipitation, while power ($P = I^2 + Q^2$) is exponentially distributed. Phase is uniformly distributed in noise but becomes correlated for weather signals, enabling the estimation of Doppler velocity. These statistical properties of radar signals are fundamental for radar moment estimation: reflectivity depends on power statistics, velocity on phase correlations, and spectrum width on I/Q decorrelation rates (Doviak & Zrnic, 2014). Deviations from these distributions occur in exceptional cases—hail produces non-Rayleigh amplitude distributions, while ground clutter causes Rician statistics. Linear dual-polarization radars transmit horizontally and vertically polarized signals. This paper deals with single-polarization radar signals.

2.1. Simulation of Radar

A weather radar signal time series of precipitation was simulated based on a specified Doppler power spectral density (Zrnić, 1975). The Doppler power density is defined by the signal-to-noise ratio, mean velocity ($\bar{v}$), and the spectrum width (σ_v) of the velocity. A Gaussian spectral model was used to simulate the weather radar time series data. The assumption of Gaussian weather spectra holds most of the time, with exceptions arising in situations such as severe turbulence, wind shear, and varying fall velocities in mixed-phase precipitation, which can lead to a non-Gaussian Doppler spectrum. To generate the radar signal time series, the square root of the Doppler power spectra was multiplied by a set of random numbers. The resulting amplitude spectra were then inverse fast Fourier transformed to produce the radar signal time series. Since the received radar signal is represented as a complex voltage, it is conveniently expressed in terms of two components: the quadrature $I(t)$ and $Q(t)$ time series, as described in Section 1.

2.2. Statistics and Auto-Correlation Function of Radar Signal

Radar signal is commonly written as,

$$X(t) = I(t) + iQ(t) \tag{1}$$

where $X(t)$ represents voltage, $I(t)$ and $Q(t)$ are time series. Power, $P = \langle I^2 \rangle + \langle Q^2 \rangle$ is exponentially distributed. For one independent sample, the power estimate has a relative error of 100%. Doppler velocity is Gaussian distributed, and the Doppler spectrum width is a chi-square (χ^2) distribution because it is derived from sums of squared Gaussian variables (Zrnic, 1979). Weather radar typically collects between 16 and 128 samples of received signals to estimate radar observations.

The autocorrelation function of the radar signal X is

$$R_x(T_s) = P_0 \ \exp\left(-\frac{T_s^2}{2\tau_c^2}\right) e^{-j2\pi f_d T_s} \tag{2}$$

where P_0 is average signal power, f_d is the Doppler frequency shift, $\tau_c = \frac{\lambda}{4\pi\sigma_v}$ is the correlation time, λ is the radar transmit wavelength, and σ_v is the spectrum width of the Doppler velocity. From the above, the auto-correction function of I and Q at lag T_s is derived as follows:

$$R_I(T_s) = \frac{P_0}{2} \exp\left(-\frac{T_s^2}{2\tau_c^2}\right) \mathrm{Cos}\left(2\pi f_d T_s\right) \tag{3a}$$

$$R_I(T_s) = R_Q(T_s) \tag{3b}$$

The typical correlation time of a weather radar signal is between 3 and 10 ms at S-band transmit frequency. Therefore, for a S-band radar at 1,000 PRF, 3 to 10 I/Q samples are correlated, depending on the value of σ_v.

3. Rationale for Radar Signal Prediction

Radar time series depend on three key parameters: mean velocity, Doppler spectrum width, and signal-to-noise ratio (SNR). A S-band pulse Doppler radar (3 GHz) at 1000 PRF detects a limited range of −25 to 25 m s^{-1} of mean velocities {500 discrete values} and Doppler spectrum widths 0–5 m s^{-1}. Doppler velocities are measured with an accuracy of 1 m s^{-1}. Assuming the velocities are quantized at 0.1 m s^{-1}, there are only $500 \times 50 = 25{,}000$ combinations of mean velocities and spectrum width. Therefore, the population of 25,000 I/Q time series is finite for a specified SNR. The finite population of time series and the autocorrelation of time series enable the prediction of radar signals.

Additionally, time series are characterized by long-term trends and short-term fluctuations. This concept is fundamental to predicting time series. The rationale for predicting time series also applies to radars that operate at other wavelengths. For instance, at the W-band, a PRT of 0.1 ms yields a larger number of time series samples within a typical τ_c of 2.5 ms at a σ_v of 1 m s^{-1} (Vivekanandan et al., 2015).

4. Artificial Intelligence and Time Series Prediction

Artificial Intelligence (AI) is a broad field that focuses on creating intelligent machines capable of performing tasks typically using ML. The ML is a subset of AI, dedicated to developing systems that can learn from data without being explicitly programmed. ML enables neural networks (NN) to identify patterns and make predictions. AI utilizes NN to learn from data and make predictions. These models are particularly adept at recognizing complex patterns and have achieved state-of-the-art performance in many tasks, including image recognition, natural language processing, speech recognition, and time series prediction. A NN is not necessarily sequential or deterministic. Instead of relying on complex central processors, NNs consist of many simple processors that primarily compute the weighted sum of their inputs from other processors (Haykin, 2009). These networks do not execute programmed instructions serially; instead, they respond in parallel to input patterns. Additionally, there are no separate memory addresses for data storage; instead, information is contained within

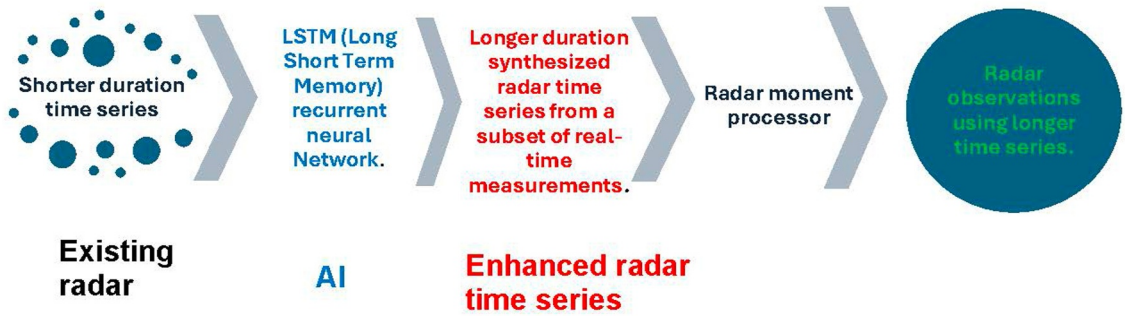

Figure 1. Overview of the conceptual process flow for artificial intelligence-based weather radar signals.

the network's overall activation state. "Knowledge" is represented by the network itself, which is greater than just the sum of its components.

Depending on the nature of the application and the strength of the internal data patterns, a network can be trained effectively. This training is beneficial for problems where relationships may be dynamic or non-linear. NNs offer an analytical alternative to conventional techniques, which are often constrained by strict assumptions of normality, linearity, and variable independence. By capturing a wide range of relationships, an NN enables users to model complex phenomena quickly and relatively easily, which may be difficult or impossible to explain using traditional methods. There are three types of learning in NN: (a) supervised learning, (b) unsupervised learning, and (c) reinforcement learning. In this paper, supervised training is used. Supervised learning is a type of learning that is guided by a supervisor, much like a teacher assisting students. In this approach, input-output pairs are used for training, where each pair consists of a set of inputs and the corresponding desired output. The model's output is compared to this desired output, and any discrepancy, referred to as an error, is calculated. This error signal is then fed back into the network to adjust the weights of the connections. This adjustment process continues until no further changes can be made, and the model's output aligns with the desired output. In supervised learning, the model receives feedback from the environment to enhance its performance.

Recurrent Neural Networks (RNNs) are designed to process and interpret time series data. In this model, the output from one processing node is fed back into the same or previous layers. The most well-known type of RNN is the Long Short-Term Memory (LSTM) network, which processes input data sequentially by iterating over time steps and updating the RNN state (Gers et al., 2000). An LSTM layer specifically learns long-term dependencies within time series and sequence data. The RNN state retains information from all previous time steps. By using prior time steps as input, an LSTM neural network predicts subsequent values in a time series or sequence. To train an LSTM neural network for time series prediction, a regression LSTM with sequence output was employed, where the target responses correspond to the training sequences with values shifted by one time step. At each time step of the input sequence, the LSTM network learns to predict the value of the next time step.

There are two methods of prediction: open-loop and closed-loop prediction. This paper focuses on the open-loop method. Open-loop prediction forecasts the next time step in a sequence using only the input data available up to that point. Predictions for subsequent time steps rely on the actual values from the data source. For example, to predict the value at time step t, the model uses the data collected from time steps 1 through $t-1$. The prediction for time step $t+1$ is made only after the actual value for time step t is recorded, using that value as input for the next prediction. Open-loop forecasting is practical when actual data is available before making the next prediction.

For I/Q prediction, the LSTM network features two separate input streams for in-phase (I) and quadrature (Q) data, which are processed through a single hidden layer consisting of 128 units. The network produces two output streams for I and Q. The hidden layer employs a gated architecture, comprising input, forget, and output gates, that effectively captures long-term dependencies. Meanwhile, the dual outputs share the same hidden state but are decoded using separate dense layers.

A conceptual process flow diagram, illustrated in Figure 1, shows how an LSTM network can be integrated into an existing radar system. Typically, the radar captures only 25% of the required time series data, while the remaining 75% is predicted using the LSTM neural network. To create a longer duration time series, the measured

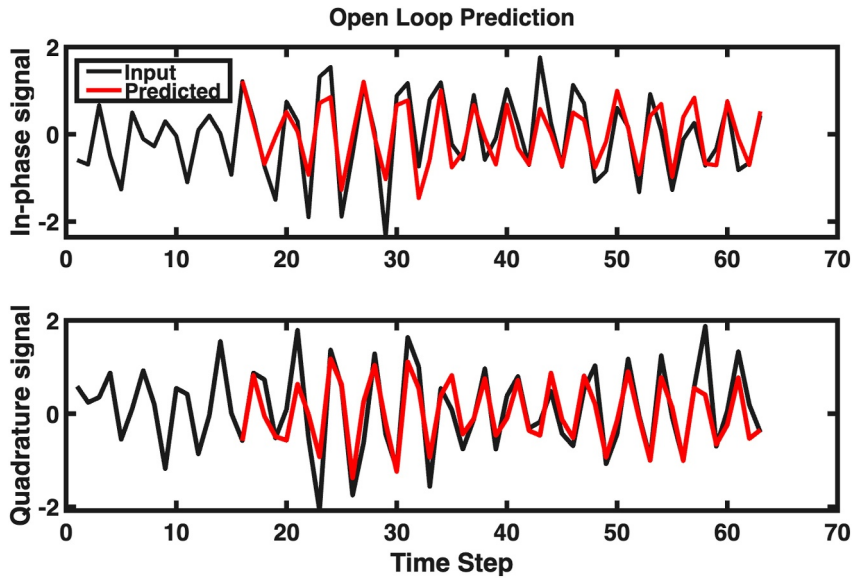

Figure 2. An example of a simulated true *I*/*Q* time series of 64 samples of duration 64 milliseconds that correspond to $\overline{v}$ = 14.6 m s^{-1} and the σ_v = 0.96 m s^{-1}. The predicted timeseries using the first 16 samples is shown in red.

25% is combined with the predicted 75% samples. The radar observations are then derived from this synthesized longer time series.

5. Prediction of Time Series

The measured *I*/*Q* time series serves as the input for a LSTM RNN. This network is designed to predict a time series of a specified length, based on training with either simulated or actual radar data. The results discussed in this paper originate from an LSTM network trained on simulated *I*/*Q* time series.

5.1. Prediction of Simulated Timer Series

To conduct the simulations, a signal-to-noise Ratio (SNR) of 10–30 dB was used, generating 10,000 pairs of *I*/*Q* time series for an *S*-band pulse Doppler weather radar. The mean velocity of the simulated data ranged from −20 to 20 m s^{-1}, and the standard deviation varied between 1 and 6 m s^{-1}. The LSTM network was trained using 90% of the simulated *I*/*Q* time series, and its performance was evaluated using the remaining 10% of the *I*/*Q* time series that were not included in the training set.

An example of a predicted time series is shown in Figure 2. The transmit frequency was 3 GHz. The time series was generated at a millisecond sample time. The LSTM network predicted 48 *I*/*Q* succeeding time series using the first 16 measured time series. The predicted timeseries is shown in red. The original time series is the black line. To quantify the accuracy of the predicted time series, pulse pair estimates using the auto-correlation function of the radar signal, $R(0)$ and $R(1)$, were employed to estimate the original 64-time series samples, and the synthesized that included the first 16 samples of the original and the subsequent 48 predicted samples. The estimated, $\overline{v}$ = 14.8 m s^{-1} was close to 14.6 m s^{-1} of the original time series. The estimated σ_v = 1.35 m s^{-1} was close to 0.96 m s^{-1} of the original time series.

The conventional approach often necessitated a substantial number of samples, typically ranging from 32 to 128, to ensure the precision and reliability of radar observations at the *S*-band (Bringi & Chandrasekar, 2001). In Figure 3, pulse pair estimates for 50 different time series are shown in scatter plots. The radar estimates on the *X*-axis in all plots were calculated from the original 64-time series. The radar estimates from the partial data (the original first 16 samples) were plotted on the *Y*-axis of the first column. The *Y*-axis of the second column is the estimates from the synthesized data.

The synthesized time series consisted of the original 16 time series, plus the predicted 48 samples. The root mean square estimate (RMSE) of the synthesized time series is lower than that of the original 16 samples.

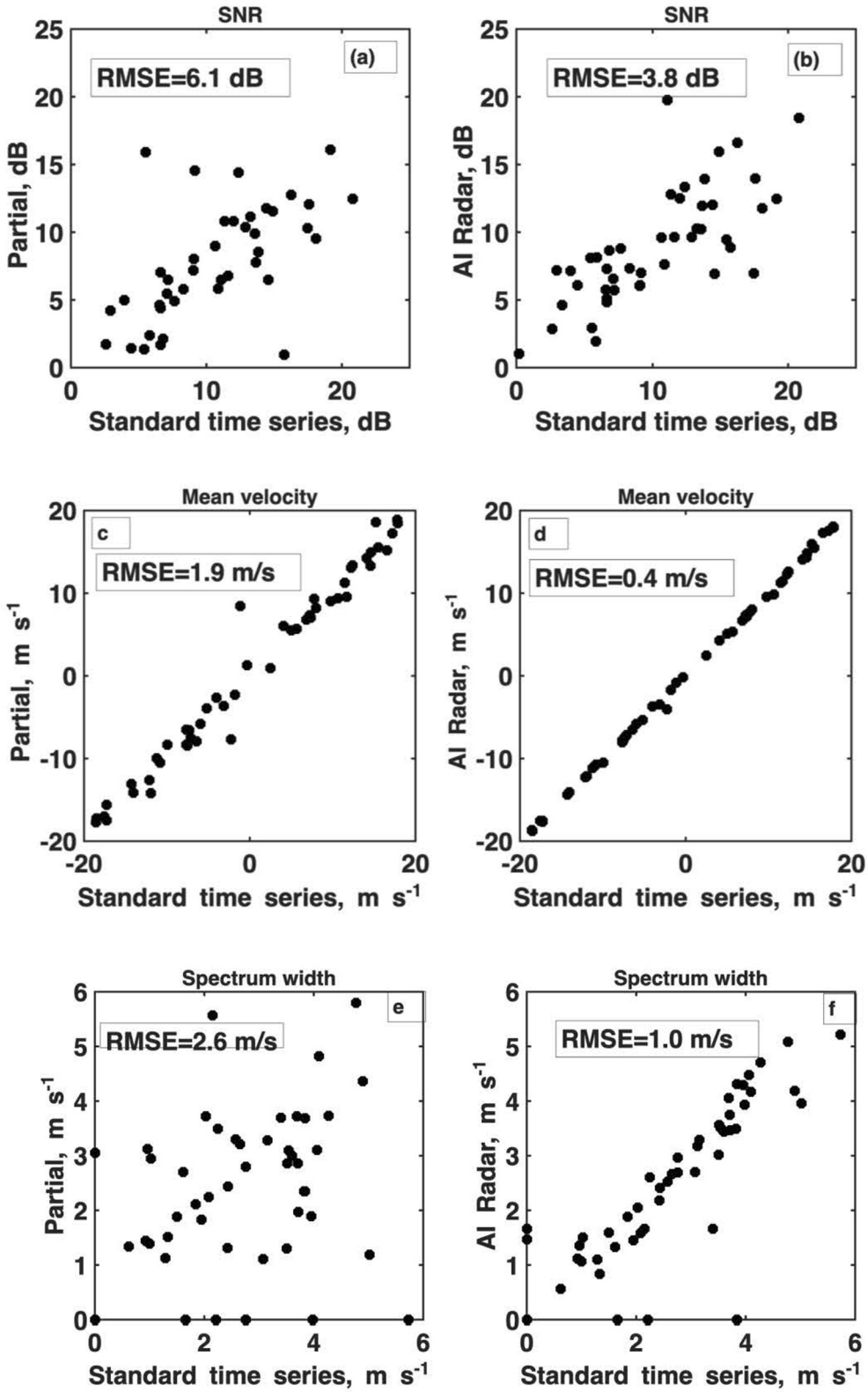

Figure 3. Displays the results for simulated time series. The reduction in Root Mean Square Error (RMSE) for (AI) radar estimations across 50 different time series is illustrated in scatter plots. The estimated Signal-to-Noise Ratio (SNR), velocity, and Doppler spectrum widths derived from 16 time series samples (a, c, and e) (partial) and AI radar (b, d, and f) are compared with standard time series estimates based on 64 samples. The partial time series estimates utilize only the first 16 time samples, while the AI radar estimate combines the original 16 samples with 48 predicted samples, resulting in a total of 64 samples.

5.2. Prediction Measured NEXRAD Time Series

The prediction technique for time series was applied to a ground-based *S*-band radar, NEXRAD. The NEXRAD KBYX, located in Key West, Florida, collected a measurement of a tropical cyclone on 28 September 2022 (NEXRAD_KBYX_2022). The KBYX long-range surveillance scan was at 0.5-degree elevation with a high PRT of 3.1 ms. KBYX measurements of a tropical cyclone reveal that the storm was greater than 250 km in size, with rainbands exhibiting reflectivity exceeding 50 dBZ and folded Doppler velocities. It is not uncommon for tropical cyclone velocities to exceed 20 m s^{-1}. Therefore, the measured Doppler velocities are folded multiple times, as the Nyquist velocity is ±8.4 m s^{-1}. No attempt was made to unfold the Doppler velocities.

Figure 4 shows radar observations from KBYX and AI radar. The AI radar was trained using the simulated *I*/*Q* data described in Section 5.1. The methodology described in the previous section was applied to predict NEXRAD time series. The surveillance scan contains more than a million *I*/*Q* samples. The LSTM NN used the initial 16-time series samples for predicting the succeeding 48-time series samples. The plots on the left column were obtained from all 64 measured samples. The middle column radar measurements used 16 measured samples and 48 predicted samples. The AI radar utilized only 25% of the measurements, and the LSTM NN predicted the remaining 75%. The third column shows the histogram of the difference between the radar measurements of the "true" values and those derived from the predicted time series.

A preliminary comparison of radar measurements between KBYX and AI radar is encouraging. Within the radar range <100 km, AI radar estimates show a good agreement with KBYX measurements. The normalized errors in the third column indicate that the peak in reflectivity error is 10%. The peak in normalized errors in Doppler velocity and spectrum is 0%. The future analysis will investigate plausible causes for bias in reflectivity measurements.

However, the proposed method can be utilized with any radar that measures *I*/*Q* time series data. This method is not restricted to a specific radar platform; it applies to ground, airborne, or spaceborne systems, as LSTM operates on *I*/*Q* signals that represent the fundamental radar measurements. Additionally, the technique is suitable for wind profilers, phased array radars, and both scanning and non-scanning radars.

6. Concluding Remarks

The AI radar system represents a groundbreaking advancement in remote sensing, integrating traditional radar measurements with ML techniques to enhance accuracy, efficiency, and resource optimization. By leveraging LSTM NN, the system predicts in-phase (*I*) and quadrature (*Q*) radar samples, effectively increasing usable sample counts without requiring extended data collection times. This approach improves measurement accuracy and resolution, reduces computational and storage demands, and enables faster data acquisition, making it particularly valuable for spaceborne, mobile, and resource-constrained radar applications.

Results from simulations demonstrate the AI radar's ability to predict radar time series, achieving a reduced root mean square error (RMSE) and close agreement with the true values. The AI radar successfully synthesized longer time series from original measurements, enhancing radar observations while maintaining statistical and spectral characteristics. Preliminary comparisons with operational radar systems, such as KBYX, show promising alignment in reflectivity, Doppler velocity, and spectrum width measurements. There was a bias between the original measured reflectivity and the predicted reflectivity using the synthesized time series. An LSTM neural network trained with simulated radar signals is unaffected by any bias present in an ideal radar receiver. Currently, we are investigating further improvements in measurement accuracy using an LSTM neural network that is trained with actual radar signals.

Future advancements could focus on addressing biases in reflectivity measurements, expanding applications to military radars, and optimizing the system for faster target detection. The AI radar's ability to reconstruct missing signal portions and adapt to various radar platforms—including ground-based, airborne, and spaceborne systems—paves the way for more agile, efficient, and adaptive radar technologies. This innovation has the potential to transform radar operations across research, operational, and specialized domains, offering significant benefits in both civilian and military applications.

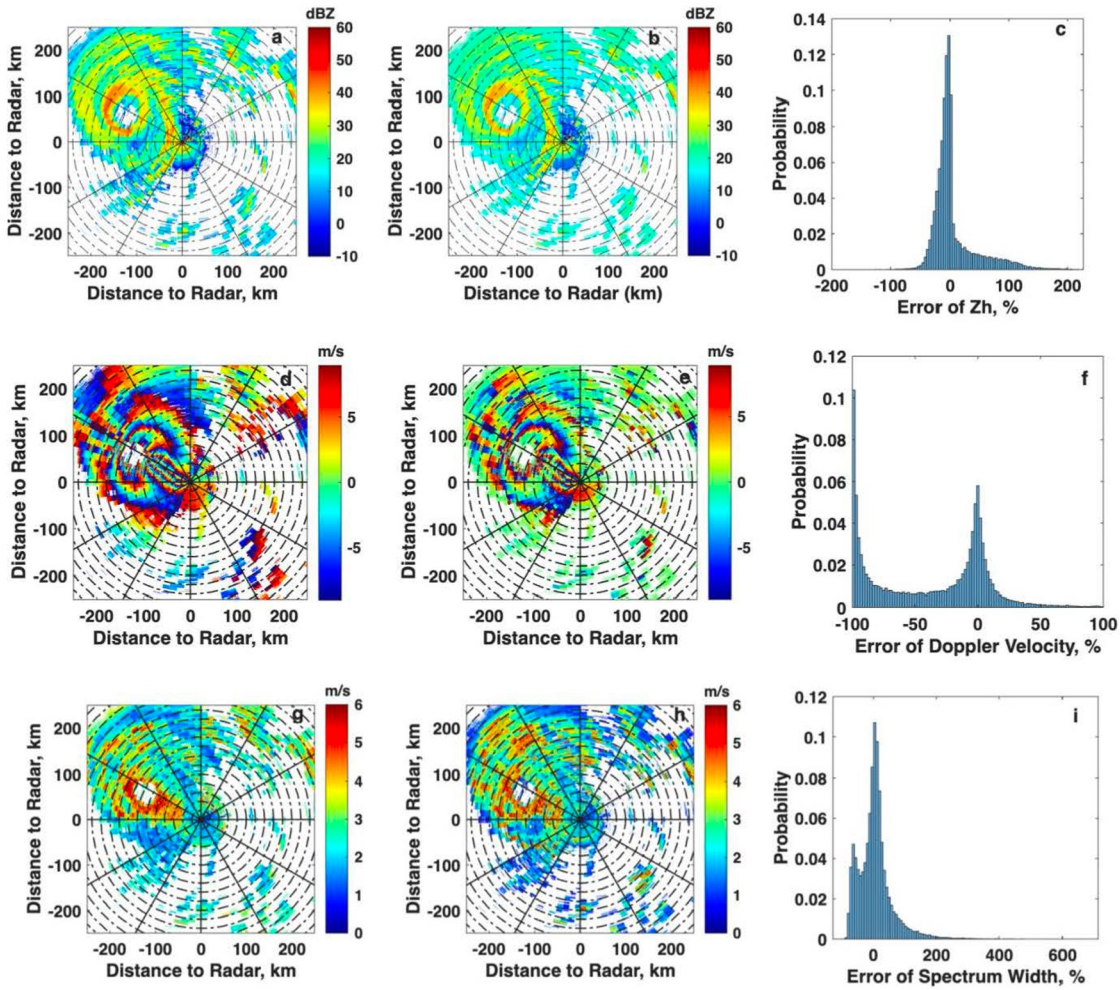

Figure 4. Compares the reflectivity, mean Doppler velocity, and spectrum width as measured by the NOAA Weather Service's operational radar (NEXRAD) and (AI) radar. The first column (a, d and g) presents data from all 64 samples collected by NEXRAD. The middle column (b, e and h) displays measurements from the AI radar, which used 16 measured samples from NEXRAD and 48 predicted samples. The third column (c, f and i) highlights the differences between the first two columns.

Conflict of Interest

The authors declare no conflicts of interest relevant to this study.

Data Availability Statement

Level II of the KBYX NEXRAD, located in Key West, Florida, collected measurements of a tropical cyclone on 28 September 2022. The radar data used in this manuscript are available at the NOAA National Centers for Environmental Information (NCEI) https://www.ncei.noaa.gov/nexradinv/displaygraphs.jsp?mm=09&dd=18&yyyy=2022&product=AAL2&filter=&id=KBYX.

Acknowledgments

The authors sincerely appreciate Eric Loew for his valuable feedback and unwavering encouragement, which significantly inspired our work on time series prediction. We would like to extend our gratitude to Prof. David Schwartzman from the University of Oklahoma, Norman, OK, for generously sharing the valuable NEXRAD data. The material is based on work supported by the National Center for Atmospheric Research, a major facility sponsored by the National Science Foundation (NSF) under Cooperative Agreement No. 1852977. Any opinions, findings, and conclusions or recommendations expressed in this material are those of the author(s) and do not necessarily reflect the views of the National Science Foundation.

References

Bringi, V. N., & Chandrasekar, V. (2001). *Polarimetric doppler weather radar: Principles and applications*. Cambridge University Press.

Crum, T. D., Alberty, R. L., & Burgess, D. W. (1993). Recording, archiving, and using WSR-88D data. *Bulletin of the American Meteorological Society*, *74*(4), 645–654. https://doi.org/10.1175/1520-0477(1993)074<0645:raauwd>2.0.co;2

Doviak, R. J., & Zrnic, D. S. (2014). *Doppler radar & weather observations*. Academic Press.

Gers, F. A., Schmidhuber, J., & Cummins, F. (2000). Learning to forget: Continual prediction with LSTM. *Neural Computation*, *12*(10), 2451–2471. https://doi.org/10.1162/089976600300015015

Haykin, S. (2009). *Neural networks and learning machines, 3/E*. Pearson Education India.

NEXRAD KBYX data. (2022). https://www.ncei.noaa.gov/nexradinv/displaygraphs.jsp?mm=09&dd=28&yyyy=2022&product=AAL2&filter=&id=KBYX

Vivekanandan, J., Ellis, S., Tsai, P., Loew, E., Lee, W. C., Emmett, J., et al. (2015). A wing pod-based millimeter wavelength airborne cloud radar. *Geoscientific Instrumentation, Methods and Data Systems*, *4*(2), 161–176. https://doi.org/10.5194/gi-4-161-2015

Zhang, G. (2016). *Weather radar polarimetry*. CRC Press.

Zrnić, D. S. (1975). Simulation of weather-like Doppler spectra and signals. *Journal of Applied Meteorology and Climatology*, *14*(4), 619–620. https://doi.org/10.1175/1520-0450(1975)014<0619:sowdsa>2.0.co;2

Zrnic, D. S. (1979). Estimation of spectral moments for weather echoes. *IEEE Transactions on Geoscience Electronics*, *17*(4), 113–128. https://doi.org/10.1109/tge.1979.294638